The kinetics of fast steps on crystal surfaces and its application to the molecular beam epitaxy of silicon

by R. Ghez S. S. Iyer

Crystal growth by molecular beam epitaxy (MBE) occurs under conditions of high supersaturation. The classic growth theory of Burton, Cabrera, and Frank (BCF) is based on the assumption that surface steps move slowly. Consequently, it requires modifications to be applicable to MBE because the velocities of surface steps may be large. In addition, because such steps are asymmetric structures, as observed experimentally by field ion microscopy, capture probabilities from above and from below a step must differ markedly. Hence the adatom concentration distribution cannot be at equilibrium at steps; there, it also suffers a discontinuity. We propose a model that treats surface step motion as a Stefan problem and that also respects its physical asymmetry. Calculations are presented which extend and complete recently published results that had

[®]Copyright 1988 by International Business Machines Corporation. Copying in printed form for private use is permitted without payment of royalty provided that (1) each reproduction is done without alteration and (2) the *Journal* reference and IBM copyright notice are included on the first page. The title and abstract, but no other portions, of this paper may be copied or distributed royalty free without further permission by computer-based and other information-service systems. Permission to *republish* any other portion of this paper must be obtained from the Editor.

imposed the restrictive condition of local equilibrium at steps. Step velocity is estimated as a function of supersaturation, degree of asymmetry, and step density. Concentration profiles are then computed; they are found to be generally skewed. In all cases, we show that the behavior of the growing crystal is convective rather than diffusive when the supersaturation is large. Consequently, we can understand the extraordinary insensitivity of the MBE of Si to changes in growth temperature and orientation.

1. Background and motivation

The crystal-growth theory of Burton, Cabrera, and Frank [1-3] explains the structure of crystal surfaces, the role of dislocations in the formation of some types of surface steps, and the rate of advance of these steps over close-packed terraces. Although not *every* crystal grows by a layer mechanism, there is now ample evidence for its relevance, for example, to epitaxial growth on vicinal semiconductor surfaces. Monoatomic steps have been detected on Si and GaAs surfaces by transmission electron microscopy [4], Nomarski phase contrast microscopy [5-8], and scanning tunneling microscopy [9, 10]. Moreover, the production of very smooth surfaces, required for submicron device processing, would be improbable if mechanisms other than

step motion were dominant. This, of course, begs the question regarding the *source* of steps. Although that question remains generally unresolved, it appears, today, that steps can originate from misorientation and crystal edges, in addition to line imperfections and edges of nuclei, as proposed by BCF.

It is, perhaps, useful to recall a simplified argument that illustrates the main assumptions of the BCF theory and that introduces relevant notation. Figure 1 shows a computergenerated surface element [11] that is composed of terraces, ledges, and kinks [12]. Atoms [13] from the volume phase come raining onto the surface with flux F. Once adsorbed on terraces, these loosely bound atoms can execute two types of jumps: to adjacent surface sites or back to the volume phase. The first type is characterized by a surface diffusivity $D_{\rm s}$, whereas a surface lifetime $\tau_{\rm s}$ describes the second. (Processes that favor adatom capture by steps are described later.) According to BCF, the product of these quantities serves to define a length scale.

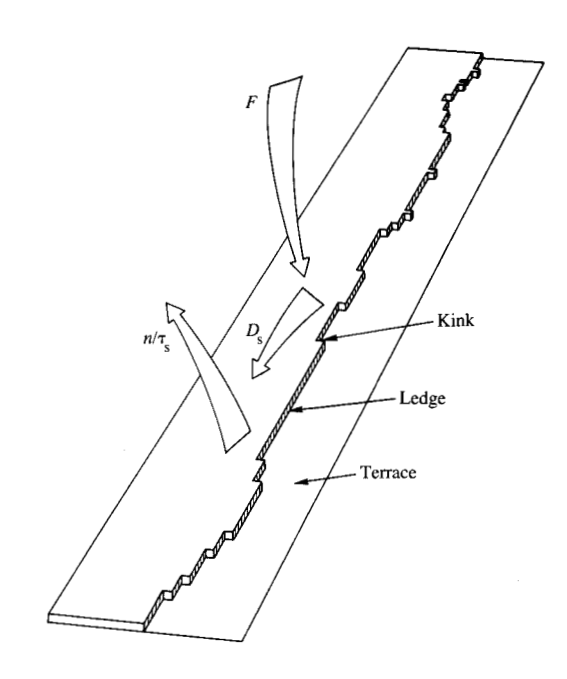
$$x_{\rm s} = \sqrt{D_{\rm s} \tau_{\rm s}},\tag{1}$$

also called the mean surface diffusion distance. This is a fundamental quantity because, in many cases, one expects surface concentration distributions n(x, t) to vary over distances of the order of x_a . Figure 2 illustrates such a distribution around an isolated step. In its immediate vicinity, the step, if it is an efficient sink [14], can maintain the concentration at its equilibrium value n_e . On the other hand, the adatom population far from the step is in equilibrium with the supersaturated volume phase. Introducing the (relative) supersaturation ratio σ and the equilibrium value F_a of the flux F, we must have the equalities $n(\pm \infty, t)/n_e = F/F_e = 1 + \sigma$. Next, if v is the step velocity and if n_r is the areal density of reticular sites, the convective flux $n_r v$ due to the motion of the step must equal the sum of the two surface fluxes $\pm D_z \partial n/\partial x$ to that step. Estimating these fluxes over the distance x_s and introducing the equilibrium coverage $\theta_e = n_e/n_r$, we easily get the BCF expression for the velocity of an isolated step,

$$v_{\infty} = 2\sigma\theta_e D_s / x_s \,, \tag{2}$$

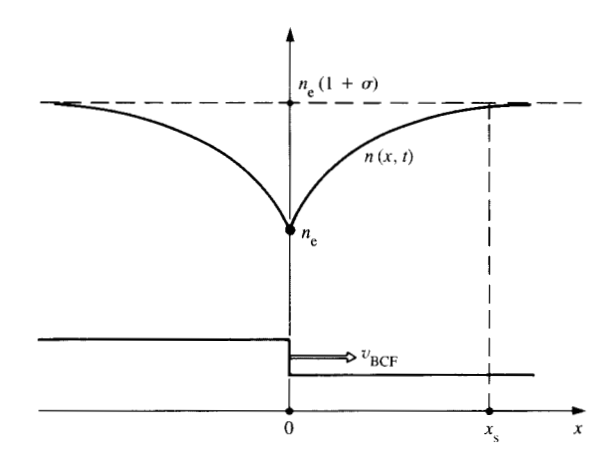
which we now briefly discuss.

First, this expression is the product of a driving force $\sigma\theta_e$ (not merely the supersaturation) and what may be called a surface diffusion velocity D_s/x_s . Thus, the question "What is a fast step?" depends on the magnitude of the dimensionless ratio vx_s/D_s , known as the Péclet number. For example, Equation (2) indicates that small driving forces imply slow steps. Second, it is evident from Figure 2 that not all of the area of the adjacent terraces is efficient for the collection of adatoms. Only the strip of width $2x_s$ (equivalent to a capture cross section) that contains a step is active. And last, it should be physically obvious that Equation (2) represents the maximum possible velocity of a step when diffusion is the



District.

Computer simulation of a growing vicinal crystal surface (courtesy of G. H. Gilmer, AT&T Bell Laboratories, cf. [11]), showing the terrace-ledge-kink structure of the surface and, schematically, the main paths for mass transport.



Schematic representation of a section through an isolated step and the adsorbed concentration distribution on the adjacent terraces. Note that here we assume local equilibrium at the step.

only transport mechanism. Additional restrictions such as competing, curved, or nonequilibrium steps will decrease this estimate. Analytically, the right-hand side of Equation (2) must be multiplied by an appropriate function f whose magnitude is less than unity. For example, BCF estimate that a train of parallel steps, spaced a distance ℓ apart, will travel at the rate

$$v_{\rm BCF} = v_{\infty} \tanh \left(\frac{y}{2} x_{\rm s} \right). \tag{3}$$

In short, the BCF theory provides estimates of crystal growth rates for monocomponent systems when steps move slowly and are efficient sinks, when steady-state conditions exist, when transport occurs by surface diffusion alone, and when volume diffusion is not rate-limiting.

Many authors have offered extensions and clarifications of the BCF theory. With no claim to completeness, we mention the important work of Chernov [15, 16] in which he introduces a "kinetic coefficient" designed to describe deviations from equilibrium at steps, as well as his treatment of macrosteps [17]. Nonequilibria were further elucidated in Temkin's random-walk calculations along ledges [18] and by Schwoebel [19], who recognized that Chernov's kinetic coefficient should depend on the direction from which adatoms approach a step. Chernov also provided the first estimate of growth-rate limitations by direct volume diffusion to steps [16]. This problem has an immediate electrostatic analog, and, consequently, its solution contains a well-known logarithmic singularity at steps. This singular behavior was removed in the work of Ghez, Gilmer, and Cabrera [20, 21], in which volume \rightarrow surface \rightarrow step transitions were required. More recently, van der Eerden has considered the combination of both these approaches [22]. There have been few attempts to model multicomponent systems. Noteworthy are the efforts of Mandel [23], Takata and Ookawa [24], and Chernov and Papkov [25, 26]. Questions relating to high coverage were addressed by Ghez [27] and by Aleksandrov and Entin [28]. The stability of step trains and their time-dependent behavior were investigated by Gilmer, Bennema, Sunagawa, and Janssenvan Rosmalen [29-31], and Müller-Krumbhaar addressed the general problem of nonuniform supersaturations [32]. Finally, the present status of the BCF theory and its position in general theories of crystal growth and habit have been admirably reviewed in monographs by Müller-Krumbhaar [33] and by Chernov [34, 35].

Close to forty years have elapsed since the original BCF publications, and, as just seen, many aspects of this theory have been thoroughly investigated. Under these circumstances, one may ask, not without reason, if this field is not closed. There is, however, one aspect of the BCF theory that merits further consideration. That theory, it will be recalled, dealt with the motion of steps under *low* supersaturations and thus with *slow* steps, slow in the sense that was discussed following Equation (2). Then, the surface

diffusion field can be computed as if steps are immobile, and their motion follows from a local mass balance argument that is used implicitly for the derivation of Equation (2). This procedure is well documented in the literature on "Stefan problems" [36]. With the advent of MBE, however, and its truly enormous operating supersaturations, it is possible that fast-moving steps are more common than generally thought. There exist at least three earlier investigations of this problem. In 1963, Mullins and Hirth [37] considered the question of an isolated fast step that is in local equilibrium, but they deemed such behavior unlikely. A few years later, in 1972, Ghez presented similar calculations for parallel step arrays that, furthermore, need not satisfy local equilibrium [38]. These results remained unpublished because MBE was then a largely unrecognized technique. More recently, Voigtlaender, Risken, and Kasper [39] analyzed the problem of step arrays, with the additional, restrictive, BCF-like proviso that steps be locally at equilibrium. (Reference [40] essentially duplicates these results.) This restriction is not at all trivial because it is known that steps are not symmetric structures with respect to attachment-detachment processes at ledges. Field ion microscopy has demonstrated unambiguously that atoms, diffusing toward a step along an "upper" terrace of a facet, are often repelled at the boundary step [41–44]. Consequently, not only should one consider potential barriers around a step that represent nonequilibrium conditions, but also, as Schwoebel had noted [19], these barriers need not be symmetric.

This paper exhumes and extends Ghez's earlier calculations [38] and presents them, it is hoped, in a form that will be useful to practitioners of MBE. They may, perhaps, even serve those who lean toward the various forms of chemical vapor deposition in those cases where intermediate surface reaction steps are fast. The main assumptions are not very different from those in the original BCF publications: steady-state conditions, equidistant straight step trains, fast diffusion in the volume phase and on ledges, an adequate density of kinks, the restriction to monocomponent systems, and, thus, no occurrence of surface reactions other than adsorption. Special care, however, will be given to the boundary conditions at a step that characterize its nonequilibrium state.

2. The diffusion-convection problem and its solution

Consider a section of a vicinal surface, as depicted in Figure 3(a). It consists, essentially, of an equidistant array of straight steps. The one-dimensional, steady-state concentration n(x) of adatoms on terraces, measured in a coordinate frame that moves with the velocity v of the steps, obeys the differential equation

$$D_{s} \frac{d^{2}n}{dx^{2}} + v \frac{dn}{dx} - \frac{n}{\tau_{s}} + F = 0.$$
 (4a)

806

Here, D_s , τ_s , and F have exactly the same meaning as previously [45]. This statement of mass conservation on terraces is identical to the BCF equation, save for the second (convective) term. There are several consequences of this form. First, it must hold for all states, including equilibrium, for which the concentration is spatially constant. Therefore,

$$n_{e} = \tau_{s} F_{e} \tag{4b}$$

is an expression of detailed balance between equilibrium values. Next, the actual impingement flux F is related to the supersaturation σ through

$$F = F_c(1 + \sigma), \tag{4c}$$

a form which, inserted into Equation (4a), is compatible with the equilibrium state $\sigma=0$. Last, multiplying Equation (4a) throughout by τ_s and remembering the definition (1), we recognize with BCF that the mean diffusion distance x_s is a natural length scale and, consequently, that the Péclet number vx_s/D_s measures the relative dominance of convection over diffusion.

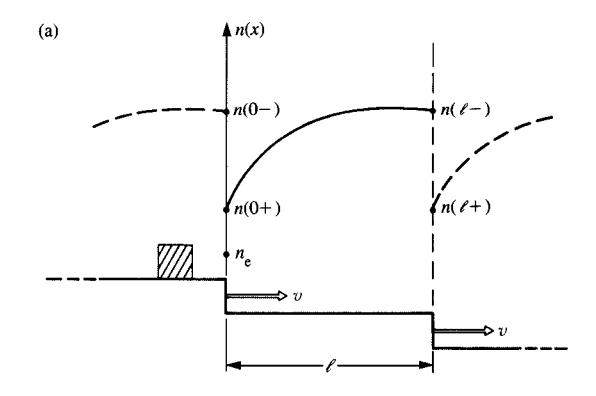
We now inquire into the boundary conditions at a given step. Figure 3(b) shows a schematic potential energy diagram for adatoms that diffuse on terraces in the periodic lattice potential. As these adatoms approach a step, however, they experience barriers that are due to the net breaking of more bonds than required for surface diffusion, and, as noted above, the barrier to the left is, most likely, higher than that to the right. In Appendix A we analyze attachment—detachment processes at ledges, and we show that these kinetics can be represented through "radiation" boundary conditions

$$\pm D_{\rm s} \frac{dn}{dx} \big|_{0\pm} = k_{\pm} [n \big|_{0\pm} - n_{\rm e}] \tag{5a, b}$$

that hold on the positive and negative sides of each step. [The notation $0\pm$ has the usual meaning of right and left limits as $x\to 0$.] Here, k_+ and k_- are the corresponding reaction constants for capture at a step; these need not be at all equal. Their values control the deviation of the adatom concentration, just below and above the step, from its equilibrium value n_e . Furthermore, we also show in Appendix A that local mass balance at a step demands the following "Stefan condition":

$$n_{\rm r}v = \left[D_{\rm s} \frac{dn}{dx} + vn\right]_0^{0+}.$$
 (6)

The problem represented by Equations (4)–(6) is formally quite simple, for we have nothing but an ordinary linear differential equation with constant coefficients (4) together with two boundary conditions (5) that are linear in concentration. On the other hand, Equation (6) will yield a transcendental equation for the step velocity v because that quantity already appears in the differential equation (4a) and, therefore, in its solution.



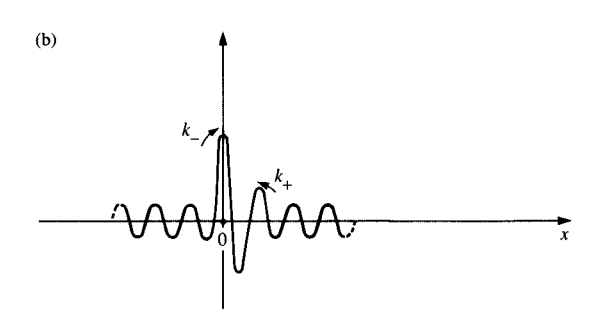


Figure 3

(a) Adatom distribution between two steps of an array. Note that the concentration is discontinuous at steps if these are not at local equilibrium. (b) Potential energy plot for adatoms in the vicinity of a step. The barriers on its left and right need not be equal, i.e., the capture rates k_+ can differ.

Before outlining this solution, it may be well to discuss the physical content of the previous equations. In the first place, Equations (4) (identical, except for notational differences, to those proposed by Mullins and Hirth [37]) are the natural extension of the BCF equations [1, 3]. The only difference resides in the convective term v dn/dx that stems from the motion of the coordinate frame. Calculations are often easiest in that frame, particularly since the velocity v is a constant for steady-state problems. Next, the rate constants k_{\perp} , in Equations (5), control deviations from equilibrium. They allow a continuous transition from local equilibrium $(k \to \infty)$ to a "blocking" condition $(k \to 0)$. In addition, as noted above, a given step is not necessarily symmetric, so that, for example, one side may be at equilibrium while the other may be blocking. In this regard, we note that the convective term of Equation (4a) introduces a further measure of asymmetry—formally, that equation is not invariant under reversals of the x-axis—which indicates

simply that, all other conditions being equal, growth and evaporation occur at different rates. And last, the reader may have noticed an important difference between the concentration distributions on Figures 2 and 3: In the latter, the *concentration*, as well as the flux, generally experiences a jump discontinuity at steps. This behavior is due to the causes of asymmetry that were just noted. Consequently, the second terms $vn|_{0_{\pm}}$ in condition (6) do not cancel except when n is anchored to its equilibrium value $n_{\rm e}$ at steps. For convenience, we now write these equations in dimensionless form.

First, in accordance with our previous remarks on the mean diffusion distance x_s , all lengths (running coordinate x, step distance ℓ , etc.) are measured in this scale, and, henceforth, primes will mean differentiation with respect to the scaled coordinate x/x_s . Next, we recognize that n/n_r is exactly the definition of the coverage θ , and Equation (4a) then becomes

$$\theta'' + (vx_s/D_s)\theta' - \theta + \theta_s(1+\sigma) = 0. \tag{7}$$

Again following BCF, this form suggests the introduction of a new unknown function

$$\psi = \sigma \theta_a - (\theta - \theta_a) \tag{8}$$

which measures deviations from the driving force $\sigma\theta_e$. It renders homogeneous the previous equation (7), and Equations (5)–(7) then become

$$\psi'' + 2V\psi' - \psi = 0. \tag{9}$$

$$\mp h_{+}\psi'|_{0+} + \psi|_{0+} = \sigma\theta_{e}$$
, (10a, b)

$$2V = [\psi' + 2V\psi]_{0+}^{0-}. (11)$$

Here, the Péclet number

$$2V = vx_s/D_s \tag{12a}$$

and the dimensionless rate constants [46]

$$h_{\perp} = D_{\epsilon}/x_{\epsilon}k_{\perp} \tag{12b}$$

compare the step's velocity v and capture-rate constants k_{\pm} to the diffusion velocity $D_{\rm s}/x_{\rm s}$ [47]. With these definitions, for example, $h_{+}=0$ and $h_{-}=\infty$ imply local equilibrium and blocking condition of a step with its leading and trailing terrace, respectively. Likewise, the BCF result (2) for isolated steps is simply $V_{\infty}=\sigma\theta_{\rm e}$. Finally, for future reference, it is convenient to define the sum and difference of these dimensionless rate constants:

$$h = \frac{1}{2}(h_{+} + h_{-})$$
 and $d = \frac{1}{2}(h_{+} - h_{-})$. (12c)

The steps were assumed equidistant. Consequently, we can now solve Equations (9)–(11) in the periodic region (0, ℓ), which means that conditions just before the step, at x = 0–, are exactly the same as those at $x = \ell$ –. It is easily verified that the general solution of Equation (9) has the form

$$\psi(x) = \frac{e^{-\nu x}}{\sinh \beta \ell} [p \sinh \beta (\ell - x) + q e^{\nu \ell} \sinh \beta x], \quad (13a)$$

where p and q are the as-yet-unknown ψ -values on either side of steps

$$p = \psi(0+)$$
 and $q = \psi(0-) = \psi(\ell-)$, (13b)

and where β stands for the abbreviation

$$\beta = \sqrt{1 + V^2}.\tag{13c}$$

This form (13a) is convenient because it expresses the arbitrary integration constants in terms of physically meaningful quantities. Now, the derivative ψ' of Equation (13a) is also linear in p and q, so that its insertion into the three conditions (10) and (11) yields a system for the three unknowns: p, q, and V. We can either solve this nonlinear system directly or, considering V as a parameter, we can take advantage of its linearity with respect to p and q [i.e., the 2×2 system of Equations (10)] to get first

$$p(\Delta/\sigma\theta_{\rm e}) = 1 + h_{-}(\beta \coth \beta \ell - V) + h_{+}\beta \frac{e^{V\ell}}{\sinh \beta \ell}, \quad (14a)$$

$$q(\Delta/\sigma\theta_{\rm e}) = 1 + h_{+}(\beta \coth \beta \ell + V) + h_{-}\beta \frac{e^{-V\ell}}{\sinh \beta \ell}, \quad (14b)$$

with the abbreviation

$$\Delta = 1 + h_{+}h_{-} + (h_{+} + h_{-})\beta \coth \beta \ell + (h_{+} - h_{-})V$$

$$= (h + \beta \tanh \frac{1}{2}\beta \ell)(h + \beta \coth \frac{1}{2}\beta \ell) - (d - V)^{2}$$
(14c)

for the determinant of the system (10). [Note the use of definitions (12c) and of the identity 2 $\cot 2z = \tanh z + \coth z$ in the second form of Equation (14c).] To get the velocity, we need only apply similar steps to Equation (11) and then eliminate p and q with Equations (14). After some algebraic manipulations, we get

$$V\left[\frac{\Delta \sinh \beta \ell}{\sigma \theta_{\rm e}}\right] = \beta (1 + 2dV)(\cosh \beta \ell - \cosh V\ell) + h(\beta - V)^2 \sinh \beta \ell + 2hV\beta(\sinh \beta \ell - \sinh V\ell), \tag{15}$$

i.e., a transcendental equation for V as a function of the physical parameters $\sigma\theta_e$, h_\pm , and ℓ . The problem is now completely solved because, from the solution of Equation (15), we determine the boundary values (14) and, therefore, the concentration through Equations (8) and (13a). We discuss this solution in the next sections.

3. Analytic content and limiting cases

We have just seen that the solution of the previous diffusion-convection problem rests entirely on the solution of Equation (15) for the velocity V. It has the form

$$V = \sigma \theta_{\rm e} f(V), \tag{16}$$

where the function f(V), always positive, also depends on the parameters h_{\pm} and ℓ [48]. On the other hand, this function is *independent* of the driving force $\sigma\theta_{\rm e}$. Does Equation (16) always have a solution, and if so, is that solution unique? We proceed heuristically by investigating the behavior of f(V) for small and large values of V. We then examine the limiting cases of small and large step distance ℓ . In all these cases we inquire into the effect of capture kinetics h_{\pm} .

We begin with a few general observations. First, we recognize that Equation (16) is precisely of the form discussed after Equation (2); namely, the (dimensionless) velocity V is the product of a driving force and of a function that describes all other reasons for change [49]. This has an immediate interpretation in terms of equivalent circuits because, graphically, the solution of Equation (16) is the intersection of the function f(V) with the straight line $V/\sigma\theta_e$. Figure 4 shows how this occurs for two different cases, to be discussed shortly, of the function f. If we think of the driving force as a voltage, and of the velocity as due to a (mass) current, then f is the analog of a (nonlinear) admittance or response function. The graphical solution is precisely its intersection with a "load line," whose slope (on a linear plot) is inversely proportional to the driving force $\sigma\theta_a$. This should not be too surprising since, after all, the diffusionconvection problem is linear. Next, we observe that our general expressions (15), (16) contain earlier-published results as special cases. In fact, if equilibrium holds on both sides of steps, $h_{+} = 0$, we obtain the result of Voigtlaender, Risken, and Kasper [39],

$$V = \sigma \theta_{\rm e} \beta \, \frac{\cosh \, \beta \ell - \cosh \, V \ell}{\sinh \beta \ell}$$

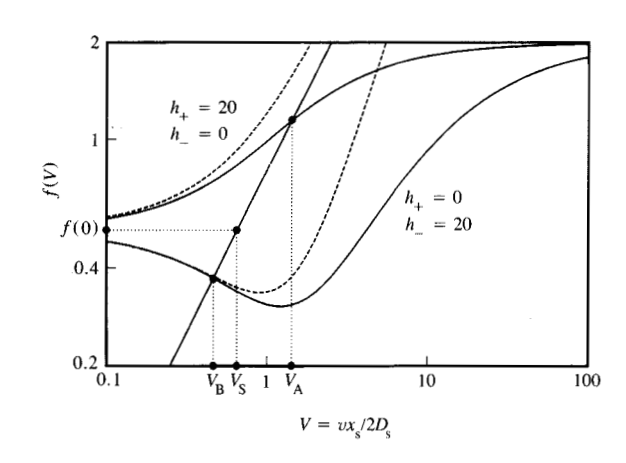
$$= \sigma \theta_{e} \beta \frac{\sinh \frac{1}{2} (\beta + V) \ell \sinh \frac{1}{2} (\beta - V) \ell}{\sinh \frac{1}{2} \beta \ell \cosh \frac{1}{2} \beta \ell}.$$
 (17)

As these authors had noted, this reduces, in the limit $\ell \rightarrow \infty$, to the expression obtained by Mullins and Hirth [37],

$$V = \sigma \theta_{o} / (1 - \sigma^{2} \theta_{o}^{2})^{1/2}$$
 (18)

for isolated steps. This expression is generalized in Appendix B when equilibrium does *not* hold at isolated steps. The last observation relates to an earlier remark, following Equation (6), regarding the physical asymmetry of the problem. If we write out, in full, the parameter dependence of the response function $f(V \mid l, h_+, h_-)$, then Equation (15) shows that f is invariant under the transformation $V \rightarrow -V, h_+ \rightarrow h_-$, and $h_- \rightarrow h_+$. Since the h's, in fact, distinguish the two sides of a given step, these substitutions show that Equation (16) is *not* invariant under equal and opposite driving forces. This asymmetry between growth and evaporation will be explored elsewhere.

We next examine the behavior of the function f for small values of V. A Taylor expansion yields



Graphical solution of Equation (16). The load line intersects two cases for the response function f(V) at points V_A and V_B . The full lines are the labeled response functions when $\ell/2x_s=2$, and the dashed lines correspond to their estimate [Equation (B3)] when $\ell\to\infty$. These two cases correspond to an asymmetric step that is essentially blocking on one side and is at equilibrium on its other side. Both solutions tend to Schwoebel's solution $V_S = \sigma \theta_e f(0)$ when the driving force is small. Increasing the driving force is equivalent to decreasing the slope of the load line. On a log-log plot, such as this one, the load line has unit slope, and an increase in driving force corresponds to its downward parallel shift.

$$f(V) = f_0 + f_1 V + O(V^2), \tag{19}$$

wher

(17)
$$f_0(\ell) = (\tanh \frac{1}{2}\ell + h)/\Delta_0$$
, (20a)

$$f_1(\ell) = 2d \tanh \frac{1}{2}\ell(h \tanh \frac{1}{2}\ell + h^2 + d^2)/\Delta_0^2,$$
 (20b)

$$\Delta_0(\ell) = (h + \tanh \frac{1}{2}\ell)(h + \coth \frac{1}{2}\ell) - d^2,$$
(20c)

and where, evidently, the determinant (20c) is exactly the expression (14c) evaluated at V = 0. The first point to notice is that Equation (16), when evaluated in the limit of very small velocities, yields exactly Schwoebel's expression [19]

$$V_{\rm S} = \sigma \theta_{\rm e} f_0 \tag{21}$$

for generally unequal capture kinetics [50]. The BCF limit (3) then emerges when equilibrium holds on both sides of all steps, i.e., when $h_{\pm} \rightarrow 0$. Thus, it should be clear that these results obtain when the load line $V/\sigma\theta_{\rm e}$ is very steep, namely, when the driving force is very small. The next point concerns the sign of f_1 in the expansion (19). This coefficient has the sign of $d=\frac{1}{2}(h_+-h_-)$ because the inequality $|d| \leq h$ is always true. For example, during growth, the condition $h_+ > h_-$ means that the trailing side of a step is closer to equilibrium than is the leading side and, therefore, that

809



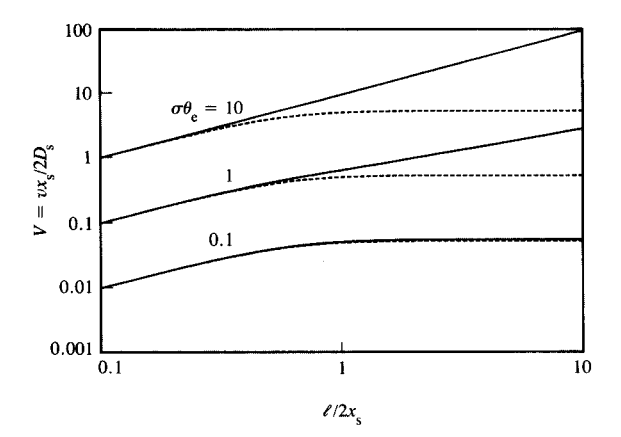


Figure 5

Velocity as a function of step distance (or misorientation) for three values of the driving force $\sigma\theta_c$. The steps are assumed at equilibrium on their left, $h_-=0$, and they suffer sluggish kinetics, $h_+=20$, on their right. The dashed lines (identical except for a parallel shift) represent Schwoebel's solution (21). This solution is evidently valid either for small values of ℓ/x_s or for small values of $\sigma\theta_c$.

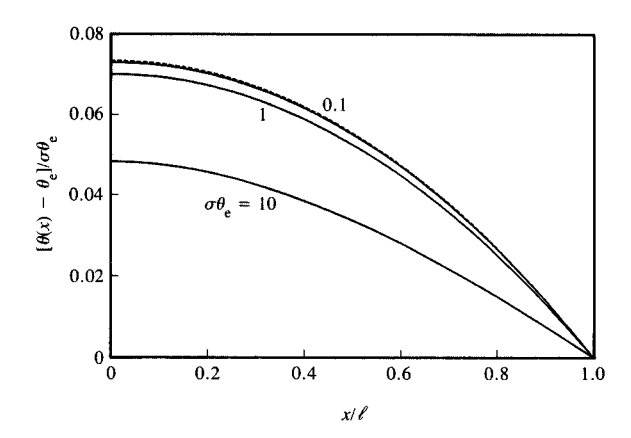


Figure 6

Normalized concentration distribution of adatoms between steps under the same supersaturation and kinetic conditions as in Figure 5. The step distance is small: $\ell/2x_s=0.2$. Note the large deviations from estimates that neglect convection (Schwoebel, dashed line) when $\sigma\theta_a\gtrsim 1$.

n(0+) > n(0-). It follows that a step, moving in the positive x-direction, encounters adatoms at high concentration levels, and that it recedes from adatoms at low levels. Thus, the

convective term in Equation (6) contributes a positive amount over the diffusion term, and we expect that the velocity, labeled $V_{\rm A}$ in Figure 4, will always be larger than Schwoebel's estimate $V_{\rm S}$. Opposite conclusions ($V_{\rm B} < V_{\rm S}$) are reached when $h_+ < h_-$, and the initial behavior (19) should be evident in the two cases shown in Figure 4. In sum, for small driving forces $\sigma\theta_{\rm c}$ we recover BCF-like results to zeroth order, with first-order corrections that depend markedly on the relative values of the capture coefficients.

On the other hand, for large velocities and finite step distance, the function f always tends toward the constant $\frac{1}{2}\ell$. More precisely, for $|V|^{-1} \ll \ell \ll 2|V|$, the asymptotic behavior of f is

$$f(V) \sim \frac{\ell}{2} \times \begin{cases} \frac{1 + 2Vh_{+}}{1 + h_{+}(h_{-} + 2V)} & \text{for } V \to +\infty, \\ \frac{1 - 2Vh_{-}}{1 + h_{-}(h_{+} - 2V)} & \text{for } V \to -\infty. \end{cases}$$
 (22)

From a practical point of view, this means that for large (positive or negative) driving forces, i.e., when the load line is very shallow, we must have the remarkably simple result

$$V \sim \sigma \theta_{\rm e} \frac{\ell}{2},$$
 (23)

regardless of step kinetics. This central result is discussed further in Section 5, but, for our purposes here, it shows that Equation (16) always has at least one solution. Moreover, in the case discussed above, $h_+ < h_-$; i.e., when the response function has a minimum in Figure 4, Equation (16) may have up to three real roots, some of which may be unstable. This question will be explored elsewhere.

Interestingly, this last estimate (23) also holds for small step distance, as a Taylor expansion in ℓ shows. For $\beta \ell \ll 1$, Equation (15) yields

$$f(V) \cong \frac{\ell}{2} \frac{h + (1 + 2dV)^{\frac{1}{2}\ell}}{h + (1 + h^2 - d^2 + 2dV)^{\frac{1}{2}\ell}} , \qquad (24)$$

and the result (22) is always valid for large velocities. Thus, for small step distance and for any driving force, the load line intersects the response function at an ordinate that is never very far from $\frac{1}{2}\ell$. In fact, one can visualize changes in ℓ as shifts, up or down, of the response function f(V), because both f(0) and $f(\infty)$ are monotonically increasing functions of ℓ . The estimates (22) and (24) also show that Equation (16) reduces, in these limits, to quadratic equations in ℓ whose physical solutions are essentially Equation (23). Rather than continue our analytic discussion, let us turn to numerical examples.

4. Graphical illustrations

The numerical solution of Equation (16) and the evaluation of the concentration distributions (8) and (13) are standard problems. In passing, although we have found it more

efficient to use the "bisection" method, Equation (16) also lends itself to a one-step iteration method, namely,

$$V_{i+1} = \sigma \theta_{\sigma} f(V_i) \qquad i = 1, 2, \cdots.$$
 (25)

Note that if the initial guess is the origin $V_0 = 0$, then Schwoebel's result (21), which holds for small enough driving force, is given precisely by the first iterate V_1 of Equation (25). In this section, we begin by examining the same physical cases that were chosen for Figure 4, namely, asymmetric steps that are at equilibrium on one side and that are essentially blocking on the other side. Next, we investigate the case of symmetric steps.

Consider first the case where exchanges with the trailing terrace occur at equilibrium $(h_{-}=0)$, but where the kinetics of exchange with the leading terrace are sluggish $(h_{+} = 20)$. Then, as predicted from Figure 4, we expect the velocity always to be larger than the estimate (21). Figure 5 displays the velocity as a function of step distance for three values of the driving force. The dashed lines correspond to Schwoebel's result (21), and we see large deviations from his estimate when the driving force and the step distance are large [51]. In fact, for $\sigma\theta_e \gtrsim 1$ we observe approximately linear behavior of the velocity, in accordance with Equation (23). The next figures show the adatom concentration distribution for two different step distances. Figure 6, for $\ell = 0.4x_s$, clearly shows a low flux condition at the right of steps and the equilibrium condition at their left. All three curves have the same qualitative behavior, but it should be noted that they differ widely, in absolute terms, because they are scaled by $\sigma\theta_{\bullet}$ in this and the next figures. As seen in Figure 7, convection begins to dominate, for large enough driving force, if the distance between steps is increased by an order of magnitude. For $\sigma\theta_e = 10$ we see that the distribution is essentially linear, and the other two curves on that figure cannot exactly maintain a low flux condition at x = 0.

The opposite case of sluggish trailing and equilibrium leading exchange kinetics $(h_{-}=20, h_{+}=0)$ is displayed in the next three figures. These should be compared to Figures 5-7. Figure 8 shows how the velocity varies with step distance and with driving force. Now, however, it is less than Schwoebel's result (21), again shown dashed, when $\sigma\theta_c < 1$. Notable differences appear, however, for larger driving forces. For example, the "dip" in the curve for $\sigma\theta_e = 10$ is closely related to the same feature in Figure 4, and the linear asymptotic behavior (23) again holds when V is large enough. [This happens, according to Equation (22), when $V \gg \frac{1}{2}h_{-} = 10$.] Figure 9, for small step distance, is almost the mirror image of Figure 6, except that the order of the curves is reversed because the leading terrace is now the more efficient supplier of adatoms. On the other hand, the case $l = 4x_s$, in Figure 10, shows that the already skewed distributions become yet more skewed when $\sigma \theta_e \gtrsim 10$. In that case the coverage exceeds unity. While our model treats the profile of the adatom distribution correctly, the physical

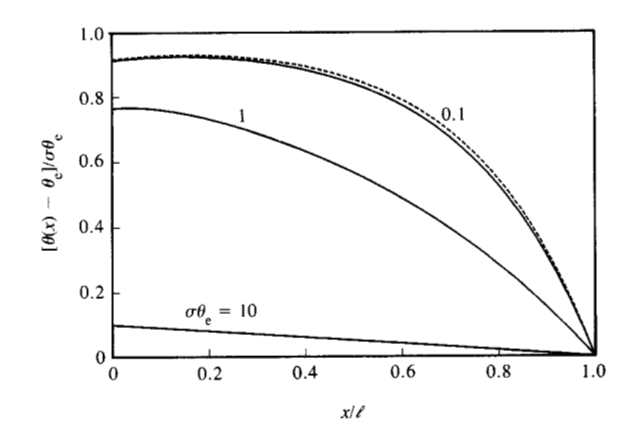


Figure 7

Same as Figure 6, but for large step distance: $\ell/2x_s = 2$.

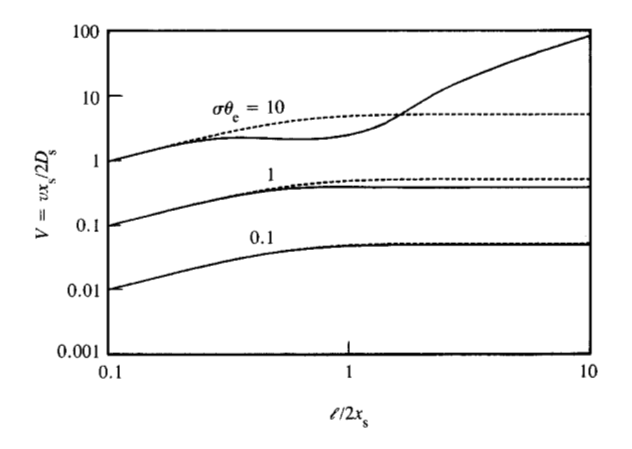
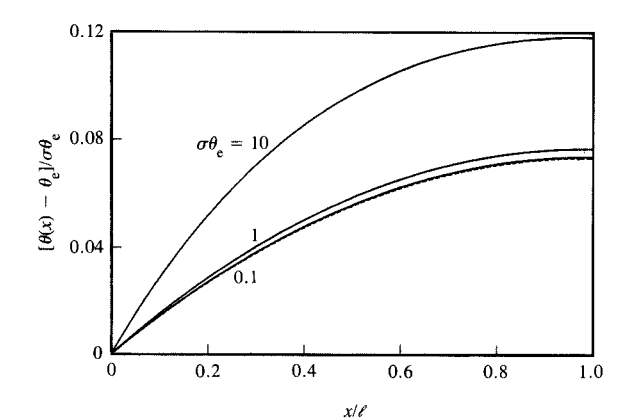


Figure 8

Step velocity as a function of step distance of asymmetric steps. The conditions are similar to those of Figure 5 except that the kinetics are reversed: $h_{-} = 20$ and $h_{+} = 0$. Note the ''dip'' when $\sigma\theta_{\rm c} = 10$ and $\ell/2x_{\rm s} \cong 1$, and the subsequent approach to linear behavior for larger ℓ

significance of this result is open to interpretation. We note the appearance of a boundary layer at x=0 because of the compromise of the concentration distribution between a fixed value ($\theta=\theta_e$) at that boundary and a fast-moving step which experiences a large convective flux. Indeed, for large V, our problem is amenable to singular perturbation techniques.





Emmess

Same as Figure 6 ($\ell/2x_s = 0.2$) except that the kinetic conditions at steps are reversed: $h_- = 20$ and $h_+ = 0$.

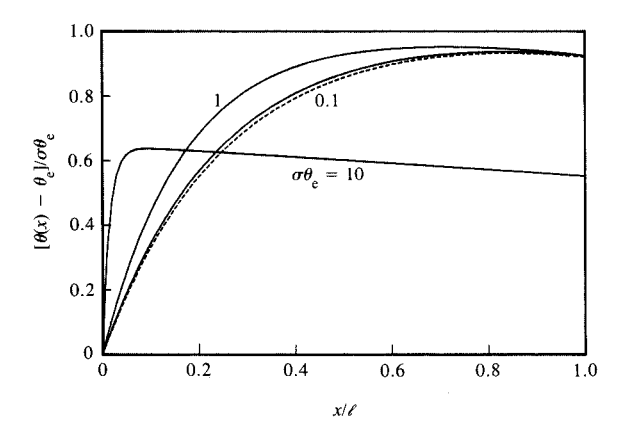


Figure 10

Same as Figure 7 ($//2x_s = 2$) except that the kinetic conditions at steps are reversed: $h_- = 20$ and $h_+ = 0$. Note the boundary layer at the leading edge that develops for larger driving forces.

All of our discussions have centered, thus far, on asymmetric steps, i.e., those for which the capture coefficients h_+ and h_- differ. Let us now consider steps that are physically symmetric; for example, take the case $h_+ = h_- = 1$. This represents steps whose capture-rate constants, from *either* side, are roughly equal to the diffusion velocity. Figure 11 shows the concentration distribution

between such steps. We note that the concentration values at the steps can deviate from equilibrium, as they should. For small driving forces, $\sigma\theta_{\rm e} \lesssim 0.1$, the distributions are symmetric, but they become increasingly skewed for larger driving forces. Consequently, concentration values on either side of steps now differ because of the additional asymmetry brought about by fast step motion. This figure thus illustrates again that there are two distinct causes of asymmetry, one due to the capture kinetics and another due to the motion of the steps themselves. In sum, unless equilibrium strictly prevails at steps, there is always a jump discontinuity in concentration at steps which contributes to the growth rate through the convective term in the Stefan condition (6).

5. Application to the growth rate of silicon by MBE, and discussion

The epitaxial growth of silicon layers by MBE is of considerable current interest because it is a low-temperature process that allows the formation of very sharp junctions [52] and the fabrication of novel structures [53–57]. Reference [58] gives an historical perspective. In this section we apply our results to this growth mode of undoped Si, but they should also apply, unchanged, to any monocomponent system.

The MBE growth kinetics of Si are remarkable. It is found, experimentally, that Si films of satisfactory crystalline perfection can be grown by MBE at temperatures below 500° C [59]. It is also agreed [60] that the growth rate is quite insensitive (<1% change) to substrate temperatures in the range $500-900^{\circ}$ C, but that it is linear with the incident silicon flux F. In fact, this flux itself is often used to calibrate the thickness of grown films in this temperature range [45]. Moreover, in this same temperature range, the growth rate appears largely independent of substrate orientation for the (100), (111), and (110) close-packed orientations and within 5° misorientation thereof.

The technological advantages of these effects are evident, and it is tempting to explain them on the basis of the Wilson-Frenkel model [61, 62]. This perhaps crudest of crystal-growth models simply postulates that almost every atom impinging on a surface will immediately incorporate into the crystal. In other words, every surface site must be a kink, and the growth rate

$$R_{\rm WF} = \Omega(F - F_{\rm e}),\tag{26}$$

where Ω is the atomic volume, is then merely proportional to the difference between the incident flux and the desorption flux from kinks. It is true, if the desorption rate is relatively small, that such a model can account for the insensitivity of the growth rate to temperature and orientation, but the high degree of crystal perfection that can be obtained by MBE demands high mobilities on smooth terraces—where there are no kinks—and it thus requires the existence of step trains. Regardless of the origin of the steps, growth then

occurs because of their motion, and BCF showed by simple kinematic considerations that the normal growth rate of the crystal R is related to the average step velocity v through

$$R = vc/\ell, \tag{27}$$

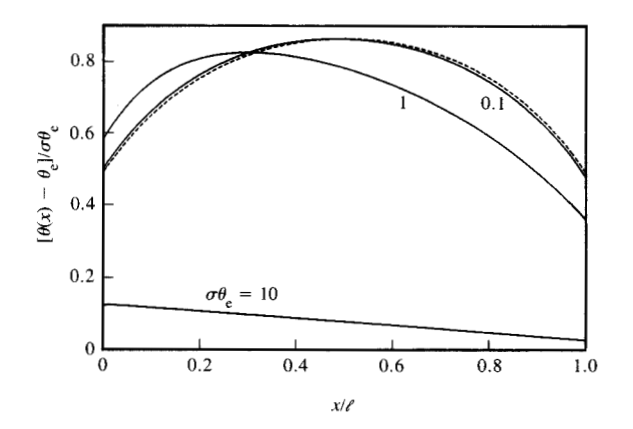
where c is the step height and where ℓ is, henceforth, the average *dimensional* distance between steps [63]. In view of Equations (12a), (16), and (27), the note in Reference [47], and the obvious relation $\Omega = c/n_{\rm r}$, we have a general expression for the growth rate

$$R = \frac{\Omega n_{\rm r} \sigma \theta_{\rm e}}{\tau} \frac{2x_{\rm s}}{\ell} f(vx_{\rm s}/D_{\rm s} | \ell/x_{\rm s}, D_{\rm s}/x_{\rm s}k_{\rm \pm}), \tag{28}$$

in which, because of Equations (4b, c), the "prefactor" $\Omega n_r \sigma \theta_e / \tau_s$ is exactly the Wilson-Frenkel growth rate (26).

But it would appear that we are impaled on the dual horns of a dilemma. First, how are we to understand a Wilson-Frenkel behavior of the growth rate, yet due to moving steps? Does this not deny rate limitations due to surface diffusion and to capture by steps? Second, as a function of misorientation [63], Equation (27) shows that the growth rate is proportional to the step velocity divided by \(\ell. \) Since all BCF-like models [3, 15, 16, 19–27] call for saturation behavior of $v(\ell)$ for small misorientations (i.e., for large ℓ ; see the dashed lines in Figures 5 and 8), it follows that none of these models can predict orientation insensitivity to growth rate, unless the average distance between steps ! always remains smaller than the mean diffusion distance x_{ϵ} . This would mean that there is a lower bound on misorientation below which the growth rate suddenly decreases. This is not observed, and we must now see whether our present calculations are, at least qualitatively, in line with observations.

There are two distinct ways in which expression (28) reduces to the Wilson-Frenkel law (26). First, if $\sigma\theta_a \lesssim 1$, then Figures 5 and 8 clearly show that the step velocity vtracks the BCF-like models. In addition, v or f increases linearly with step distance if $\ell \ll x_s$, and Equation (28) reduces to Equation (26). This is a well-known result that is expressed analytically in Equation (24). From a physical point of view, adjacent steps that are sufficiently close [51] can ensure an adequate supply of kinks, regardless of the other kinetic limitations of the adsorbate, i.e., independently of the values of the kinetic coefficients k_{\perp} . But there is also a second way in which Equation (28) reduces to the Wilson-Frenkel law. We note on Figures 5 and 8 an essentially linear dependence $v(\ell)$ for almost all step distances when $\sigma\theta_a$ is large enough. This too occurs independently of the details of adatom capture kinetics. We have seen this result, analytically, in Equations (22) and (23). From a physical point of view, a fast-moving step sweeps up all adatoms on adjacent terraces, whether or not these atoms diffuse significantly or incorporate sluggishly. Kinks in fast-moving steps are therefore just as effective for capture as a



Normalized concentration distribution for symmetric, mildly nonequilibrium steps: $h_- = h_+ = 1$. Note the skew that develops with increasing $\sigma\theta_e$ and the jump discontinuity in concentration at the steps. This latter is absent for Schwoebel's model (dashed line).

completely kinked surface or one containing closely spaced steps. In other words, as the driving force increases, the Stefan problem associated with the motion of steps becomes largely convective rather than diffusive in character.

Both of these cases are represented schematically in Figure 12. Part (a) shows how the step velocity depends on misorientation when the driving force is either small or large; it should be compared to Figures 5 and 8. Figure 12(b) shows how the growth rate depends on these same parameters. For small $\sigma\theta_e$, the velocity saturates [cf. Equation (20a)] at a value $f_0(\infty) = (1+h)/[(1+h)^2 - d^2]$, which depends on kinetics at steps. Then, the limit of Wilson-Frenkel behavior occurs when $\ell \cong x_s$, but a sharper estimate also depends on the values of capture-rate constants at steps [29]. On the other hand, for large $\sigma\theta_e$ the behavior of the velocity is essentially linear, and $R \cong R_{WF}$ for almost all ℓ , regardless of the values of k_+ .

Our view of the MBE growth of Si may be questioned because of recent RHEED intensity oscillation studies [64, 65], although certain details of image interpretation (in particular, dependence of monolayer or bilayer growth mode on the beam azimuth) remain unclear [66]. These authors suggest that growth occurs by repeated two-dimensional nucleation. It should be noted, however, that RHEED oscillations occur mainly at temperatures well below the usual conditions for MBE growth, and that a high-temperature pretreatment of buffer layers is often necessary. In other words, the surface must be somehow "prepared," perhaps precisely by creating step trains. In addition, even if the nucleation *rate* is a significant factor, the motion of

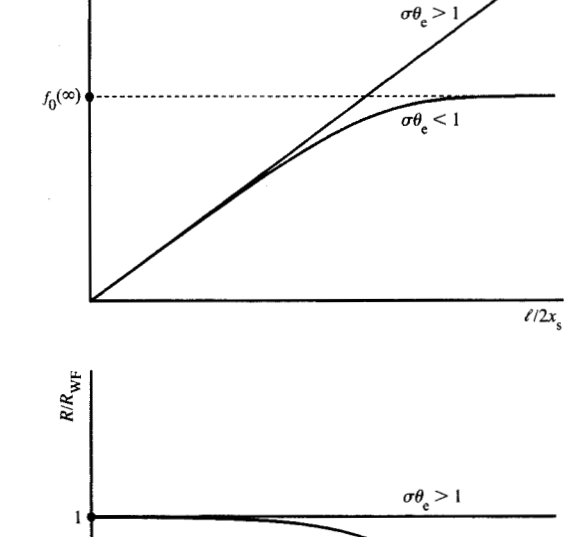


Figure 12

η/Oθ

Schematic behavior (a) of the velocity $vx_s/2D_s\sigma\theta_e$ and (b) of the growth rate R/R_{WF} as a function of step distance $\ell/2x_s$. (All variables are normalized.) The Wilson–Frenkel law is clearly always obeyed when the distance between steps is small enough. It also holds, regardless of step distance, when the driving force is large enough.

 $\ell/2x_s$

competing nuclei edges—which are steps—must also contribute to the observed growth rate. This motion, too, will be fast if $\sigma\theta_e$ is large.

It is pertinent to comment on the predictive power (and limitations) of the growth theory formulated in this paper. From an applications standpoint, our interest also clearly lies in delineating useful regimes of crystal growth. Toward that end, a short digression on numerical estimates is now needed. All along we have seen that the driving force $\sigma\theta_e$ [67] is an essential physical parameter, together, of course, with the mean diffusion distance x_s . We emphasize again that this driving force for MBE growth is not merely the supersaturation σ , but rather it is the product of the actual flux imbalance σ and the surface's "receptivity" θ_e to adsorbed atoms. With Equations (4b, c), we also have its expression $\sigma\theta_e = (\tau_s/n_t)(F - F_e)$ as the ratio of the net flux to

the maximum conceivable desorption flux, i.e., from a completely flat, singular surface. Further, as is well known [1, 3, 16, 18], τ_s , D_s , n_e , and hence x_s , and F_e can be estimated for materials whose cohesive properties depend mainly on pair interactions. These estimates are collected in Appendix C. Such a description, if applied to silicon [35, 39, 40, 59, 60]—and this may not be valid—indicates that certain low-temperature MBE conditions would yield very large values of $\sigma\theta_{\bullet}$. At T = 600°C, for example, Equations (C4) and (C5) show that a typical flux $F = 2 \times 10^{15} \text{ cm}^{-2} \text{s}^{-1}$ would produce an enormous supersaturation $\sigma \cong 1.5 \times 10^{11}$ which is evidently orientation-independent. Then, using Equation (C2), $\sigma\theta$, would be approximately 200 and 0.007 for the (100) and (111) orientations, respectively [68], because of the strong orientation dependence of the equilibrium coverage. Under these conditions, with Equation (C6), x_s would be of the order of 1.3×10^5 and 800 times the jump distance a for the same (100) and (111) orientations, respectively. On the other hand, there is no simple way to estimate the capture coefficients k_{\perp} because these depend on the detailed structure of a step [18] and on the averaging process (cf. Appendix A) necessary for a one-dimensional calculation.

These numbers, even if not accurate, are suggestive. First, growth on the Si(111) orientation probably occurs through the motion of slow steps because $\sigma\theta_e$ is small for most MBE conditions. One would expect orientation sensitivity at low enough misorientation angles. In that case, small changes in the local step density imply changes in the step velocity. Step trains could bunch and be more easily pinned by impurities [4]. Studies of growth kinetics on this orientation, however, are more likely to illuminate the details of adatom kinetics. In contrast, the (100) orientation supports large driving forces: Steps move quickly, the growth rate is more stable, and the exposed terraces are less prone to contamination. This orientation, as is observed experimentally, hosts epitaxial layers of higher quality, although carbon contamination and dislocation generation cannot be ruled out [69].

Summarizing, we have shown that if the growth of Si by MBE occurs through the motion of steps, there exist growth conditions for which these steps move at velocities that are large compared to the diffusion velocity on terraces. Under these circumstances, the overall growth rate is largely independent (1) of the temperature of the substrate, (2) of the orientation of the substrate, and (3) of the details of capture kinetics at steps. In addition, we would expect that fast step trains, in a clean environment, are relatively stable toward perturbations of the distance between steps. It follows, however, that other mechanisms that pin or retard step propagation cause a decrease in crystal quality, even when the driving force is large. This can occur either because of unintentional contamination (mainly SiC microcrystallites) or because of interference by a dopant adlayer. Practitioners

of MBE would agree today that atomically clean starting surfaces and an impeccable vacuum during growth are essential. In addition, it is well known that high dopant concentrations (mainly Ga and Sb) can severely degrade crystal quality. Extensions of our model are thus required to treat both the stability of fast step trains and the effects due to an adsorbed second component. Finally, because the surfaces of most semiconductors undergo reconstructions which persist during growth, and because these reconstructions involve substantial numbers of surface atoms, a complete theory of MBE growth would have to account, not only for adatom kinetics on these surfaces, as does this paper, but also for the continuous transformation of the surface structure into the bulk crystal structure.

Appendix A: Boundary conditions at steps

Here we outline the proof of the Stefan condition (6). Next, we justify the boundary conditions (5). Consider a step, shown schematically in Figure 13, and a laboratory coordinate frame (x, y, z) with its unit vectors (i, j, k). If $n_s(x, y, t)$ and $n_l(y, t)$ are the surface and ledge densities of adatoms, and if J_v , J_s , and J_l are the volume, surface, and ledge diffusion fluxes, respectively, mass conservation in any continuous region of the terraces and ledges demands that

$$\frac{\partial n_{s}}{\partial t} = -\nabla \cdot \mathbf{J}_{s} - \mathbf{k} \cdot \mathbf{J}_{v}|_{z=0}. \tag{A1}$$

$$\frac{\partial n_l}{\partial t} = -\nabla \cdot \mathbf{J}_l - \mathbf{i} \cdot \mathbf{J}_s \big|_{\text{left}}^{\text{right}}.$$
 (A2)

Furthermore, if (ξ, η) are the coordinates of a kink moving at velocity $v_k = \dot{\eta}$ due to attachment, there, of adatoms, then the position of the step increases by one unit a in the x-direction whenever a kink passes the origin of coordinates. This implies a normal step velocity

$$v = v_k a/\ell_k \,, \tag{A3}$$

where 4 is the average distance between kinks.

Consider now the number of adsorbed particles N_a in an arbitrary, fixed region $\mathfrak D$ that instantaneously encloses a kink. That region, however, is the union of two regions whose boundaries do move. For example, $\mathfrak D_1$, the region to the left of the step, is bounded by the fixed line $\mathcal S_1$ and by the kinked edge $\mathcal S_l$ that moves upward in Figure 13. We then have

$$N_{\mathbf{a}}(t) = \int_{\mathcal{D}_1 \cup \mathcal{D}_2} n_{\mathbf{s}} \, dx dy + \int_{\mathcal{S}_1} n_{\mathbf{l}} \, dy, \tag{A4}$$

and there are two different ways to evaluate the time rate of change N_a . First, that number changes because of all sources, interior to \mathfrak{D} , and because of all fluxes along the boundaries of \mathfrak{D} and \mathcal{S}_l . Second, one differentiates Equation (A4) directly, taking moving boundaries into account and using

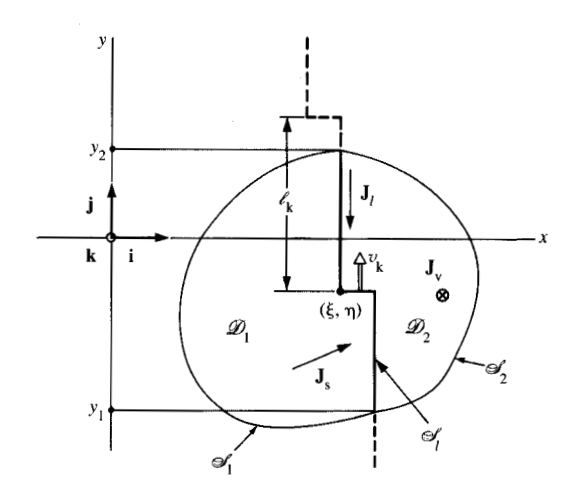


Figure 13

Plan view of a step and a kink, coordinate system, and domains for the mass balance calculations of Appendix A. The fixed domain $\mathcal{D} = \mathcal{D}_1 \cup \mathcal{D}_2$ encloses a single kink. The fluxes $\mathbf{J}_v, \mathbf{J}_s$, and \mathbf{J}_i are all directed toward their respective sinks: terrace, ledge, and kink.

Equations (A1) and (A2), together with the divergence theorem. Comparing these two procedures, we get the expression

$$[v_k n_l - \mathbf{j} \cdot \mathbf{J}_l]_{y=\eta-}^{\eta+} + \int_{\xi}^{\xi+a} v_k n_s \Big|_{y=\eta-}^{\eta+} dx = r, \tag{A5}$$

where r represents the reaction rate (the kink is a sink) of the reaction, adatom \rightarrow crystal, at kinks. This expression is nothing more than a local mass balance of the adsorbate around kinks. A second expression arises from counting the number of atoms in the crystalline phase. This number, evaluated over \mathfrak{D} , is simply

$$N_c(t) = \text{const.} + (\eta - y_1)/b, \tag{A6}$$

where b represents the size of an adatom in the y-direction and where y_1 is the coordinate of the "lower" intersection of the boundary of \mathcal{D} with the y-axis. Again, measuring its rate of change because of the reaction step r, and differentiating Equation (A6), we get the mass balance law at kinks

$$r = v_{k}/b. (A7)$$

Eliminating r between Equations (A5) and (A7), and recognizing that the integral in (A5) can be approximated, we obtain the result

$$v_{k}/b = [v_{k}n_{l} - \mathbf{j} \cdot \mathbf{J}_{l} + av_{k}n_{s}(\xi, y, t)]_{v=n-}^{n+}.$$
 (A8)

In many cases, however, one may be more interested in the

815

average behavior of the distributions n_s and n_l , rather than in a detailed two-dimensional computation. This is particularly true if ledge diffusion and kink capture are fast processes. Consequently, we define the averages in the γ -direction as

$$\bar{n}_{s}(x, t) = \ell_{k}^{-1} \int_{y_{1}}^{y_{2}} n_{s} dy$$
 (A9a)

and

$$\bar{n}_l(t) = l_k^{-1} \int_{y_1}^{y_2} n_l \, dy,$$
 (A9b)

where the distance $y_1 - y_2$ is chosen equal to the periodic interkink distance ℓ_k . Using the basic equations (A1) and (A2), we find that the averaged quantities satisfy similar relations, namely,

$$\frac{\partial \bar{n}_{s}}{\partial t} = -\frac{\partial \bar{J}_{s,x}}{\partial x} - \bar{J}_{v,z}|_{z=0}, \tag{A10}$$

$$\frac{d\bar{n}_l}{dt} = \ell_k^{-1} [v_k n_l - J_{l,y}]_{\eta^+}^{\eta^+} - \bar{J}_{s,x} |_{\text{left}}^{\text{right}}. \tag{A11}$$

Now, if it is assumed that the averaged ledge distribution is approximately at steady state, one can use Equation (A11) to eliminate the jump discontinuity of n_l and $J_{l,y}$ from the Stefan condition (A8). Further, the jump in n_s at a kink can represent its average jump along a step if the y-dependence of n_s is weak. Finally, remembering Equation (A3) and that the reticular density n_r is precisely 1/ab, we obtain the averaged Stefan condition

$$n_r v = \left[v \bar{n}_s - \bar{J}_{s,x} \right]_{\text{left}}^{\text{right}}. \tag{A12}$$

All the previous results are independent of constitutive relations. For example, nowhere was Fick's law for the various \mathbf{J} 's [e.g., $\mathbf{J}_s = -D_s \nabla n_s$] ever invoked. Of greater importance, perhaps, are the analytic expressions of the flux near boundaries. For example, our analysis in Equations (4) manifestly assumes that the exchange flux $-\mathbf{k} \cdot \mathbf{J}_v$ on terraces has the form of a first-order process $F - n_s/\tau_s$. The same can be assumed for exchanges between terraces and ledges, thus leading to the phenomenological relations on either side of steps,

$$-\mathbf{i} \cdot \mathbf{J}_{s}|_{+} = k_{s+} n_{s}|_{+} - n_{l} / \tau_{l+}$$
 (A13a, b)

Here, for example, $1/\tau_{l+}$ is proportional to the transition rate of adatoms from the ledge to immediately adjacent positions on the terrace to its right. Relations such as Equation (A13) can be understood on the basis of nonequilibrium thermodynamics of surfaces [70]. The four coefficients $k_{s\pm}$ and $\tau_{l\pm}$ are not independent because the fluxes (A13) vanish at equilibrium, and we obtain "partitioning"

$$n_{le} = \tau_{l+} k_{s+} n_{se} \tag{A14}$$

in a manner similar to Equation (4b). If, now, we assume

that the edge distribution n_t is never very different from equilibrium, then, using Equations (A14), the boundary conditions (A13) express the exchange fluxes in terms of differences between n_s and the equilibrium value n_e . This is precisely what we have expressed in Equations (5) if by n(x) we understand the quasi-steady-state spatial average of $n_s(x, y)$. In the same way, we can correlate Equation (A12) and the Stefan condition (6).

Appendix B: Isolated nonequilibrium steps

If steps are far apart, then one should get their behavior, in the limit $\ell \to \infty$, from the results of Section 2. It is easier, however, to solve the problem anew. Here, we outline this solution

If $r_{\pm} = -V \pm \beta$ are the roots of the characteristic polynomial, $r^2 + 2Vr - 1 = 0$, associated with the differential equation (9), then

$$\psi(x) = \begin{cases} pe^{xr_{-}} & \text{for } x > 0, \\ qe^{xr_{+}} & \text{for } x < 0, \end{cases}$$
 (B1)

where β , p, and q have the same meaning as in Section 2. Furthermore, because $r_+r_-=-1$, it follows that the "decay lengths" (in dimensional form) of the exponentials are $x_s r_\pm$. Thus, for growth $(\sigma\theta_e>0)$, the concentration distribution tends to sharpen in front of a moving step and to flatten on its trailing side, and conversely for evaporation. Inserting Equation (B1) into boundary conditions (10), (11) yields, first.

$$p = \frac{\sigma \theta_{\rm e}}{1 + h_{+}(\beta + V)},\tag{B2a}$$

$$q = \frac{\sigma\theta_{\rm c}}{1 + h \left(\beta - V\right)},\tag{B2b}$$

and then an equation of the form (16), with

$$f(V) = \frac{1}{2} \left[\frac{\beta - V}{1 + h_{+}(\beta + V)} + \frac{\beta + V}{1 + h_{-}(\beta - V)} \right].$$
 (B3)

This, we note, increases without bound as $V \to \pm \infty$. The function (B3) is shown as dashed lines on Figure 4. In the case of step equilibrium we get $f(V) = \beta$, and we recover the result obtained by Mullins and Hirth (18).

Appendix C: Vapor pressure and derived parameters

Here, we collect some results that are useful in estimating the parameters of our model. First, from the kinetic theory of gases and the principle of detailed balance, we express the equilibrium flux of Si as

$$F_c = p_c / \sqrt{2\pi mkT} \tag{C1}$$

in terms of its equilibrium vapor pressure p_e and its mass m; kT has its usual meaning. Next, from simple bond arguments [1, 3, 35] we have the Arrhenius behavior,

$$n_{\rm e} = n_{\rm r} e^{-W_{\rm s}/kT} \tag{C2}$$

and

$$1/\tau_{s} = \nu e^{-W_{s}'/kT},\tag{C3}$$

for the equilibrium adatom concentration and its desorption probability. The activation energies W_s and W_s' represent barriers for kink-to-terrace and terrace-to-vapor transitions, respectively, and ν is the frequency of normal vibrations. These three quantities are related through Equation (4b); hence

$$F_e = n_r \nu e^{-W/kT},\tag{C4}$$

where $W = W_s + W_s'$ is the sublimation energy. Neither W nor the product $n_r \nu$ should depend on orientation, but the latter is probably temperature-dependent. Indeed, vapor pressure data reported by Honig and Kramer [71] show no indication of deviation from purely Arrhenius behavior, and $p_e(T)$ has a sublimation energy W of 4.61 eV and a pre-exponential of 2.4×10^{10} torr [65]. Therefore, combining Equations (C1) and (C4), we must have

$$n_{\rm r}v = F_0 \sqrt{T_m/T},\tag{C5}$$

where $T_{\rm m}=1685~{\rm K}$ is the melting point of Si and where the reference flux $F_0=3.88\times 10^{30}~{\rm cm}^{-2}{\rm s}^{-1}$ is estimated from the "pre-exponential" term of the vapor expression for the vapor pressure. The equilibrium flux (C4) is thus entirely determined. If $W_{\rm s}$ is estimated from bond-breaking $[\frac{1}{2}~{\rm and}~\frac{1}{3}~{\rm of}~W~{\rm for}$ the (111) and (100) orientations, respectively], then we can also estimate both the equilibrium coverage, according to Equation (C2), and the driving force $\sigma\theta_{\rm e}$. Finally, if the activation energy U of the surface diffusivity is known (1.3 eV, according to recent measurements [72, 73]), Equation (1) yields the estimate

$$x_{s} \cong ae^{(W-W_{s}-U)/2kT} \tag{C6}$$

for the mean diffusion distance.

References and notes

- W. K. Burton and N. Cabrera, Discuss. Faraday Soc. 5, 33, 40 (1949).
- 2. F. C. Frank, Discuss. Faraday Soc. 5, 48 (1949).
- W. K. Burton, N. Cabrera, and F. C. Frank, *Phil. Trans. Roy. Soc. (Lond.) A* 243, 299 (1951).
- H. C. Abbink, R. M. Broudy, and G. P. McCarthy, J. Appl. Phys. 39, 4673 (1968).
- M. Shimbo, J. Nishizawa, and T. Terasaki, J. Cryst. Growth 23, 267 (1974).
- J. Nishizawa, H. Tadano, Y. Oyama, and M. Shimbo, J. Cryst. Growth 55, 402 (1981).
- 7. E. Bauser and H. Strunk, J. Cryst. Growth 51, 362 (1981).
- 8. E. Bauser and K. S. Löchner, J. Cryst. Growth 55, 457 (1981).
- H. J. Scheel, G. Binnig, and H. Rohrer, J. Cryst. Growth 60, 199 (1982).
- R. S. Becker, J. A. Golovchenko, E. G. McRae, and B. S. Swartzentruber, *Phys. Rev. Lett.* 55, 2028 (1985).
- 11. This unpublished Monte Carlo simulation was provided by G. H. Gilmer (AT&T Bell Laboratories). He and Ghez presented

- it at the Second European Conference on Crystal Growth (Lancaster, U.K., September 10-15, 1979) in connection with a discussion of the effect of ledge diffusion on step dynamics.
- 12. A "step" is here understood as a one-dimensional configuration composed of ledges and kinks, much as a (vicinal) "surface" is composed of terraces and steps.
- 13. The word "atoms" is used generically in the sense of any growth
- 14. Steps are efficient sinks if either edge diffusion is fast or the kink density is high. Attachment-detachment fluxes at ledges then balance approximately (cf. [11]).
- 15. A. A. Chernov, Sov. Phys. Crystallog. 1, 88 (1956).
- 16. A. A. Chernov, Sov. Phys. Uspekhi 4, 116 (1961).
- I. M. Lifshits and A. A. Chernov, Sov. Phys. Crystallog. 4, 746 (1959).
- 18. D. E. Temkin, Sov. Phys. Crystallog. 14, 179 (1969).
- 19. R. L. Schwoebel, J. Appl. Phys. 40, 614 (1969).
- G. H. Gilmer, R. Ghez, and N. Cabrera, J. Cryst. Growth 8, 79 (1971).
- 21. R. Ghez and G. H. Gilmer, J. Cryst. Growth 21, 93 (1974).
- J. P. van der Eerden, in Modern Theory of Crystal Growth I,
 A. A. Chernov and H. Müller-Krumbhaar, Eds., Springer-Verlag, Berlin, 1983, pp. 113–144.
- 23. G. Mandel, J. Chem. Phys. 40, 683 (1964).
- M. Takata and A. Ookawa, J. Cryst. Growth 24/25, 515 (1974);
 42, 35 (1977).
- A. A. Chernov and N. S. Papkov, Sov. Phys. Doklady 21, 300 (1976).
- A. A. Chernov and N. S. Papkov, Sov. Phys. Crystallog. 22, 18 (1977).
- 27. R. Ghez, J. Cryst. Growth 22, 333 (1974).
- L. N. Aleksandrov and I. A. Entin, Phys. Stat. Sol. (a) 39, 327 (1977).
- P. Bennema and G. H. Gilmer, in Crystal Growth: An Introduction, P. Hartman, Ed., North-Holland Publishing Co., Amsterdam, 1973, pp. 262-327.
- R. Janssen-van Rosmalen and P. Bennema, J. Cryst. Growth 32, 293 (1976).
- 31. I. Sunagawa and P. Bennema, J. Cryst. Growth 46, 451 (1979).
- 32. H. Müller-Krumbhaar, J. Cryst. Growth 44, 135 (1978).
- H. Müller-Krumbhaar, in Current Topics in Materials Science, Vol. 1, E. Kaldis, Ed., North-Holland Publishing Co., Amsterdam, 1978, pp. 1–46.
- A. A. Chernov, in Crystal Growth and Characterization, R. Ueda and J. B. Mullin, Eds., North-Holland Publishing Co., Amsterdam, 1975, pp. 33-52.
- A. A. Chernov, Modern Crystallography III: Crystal Growth, Springer-Verlag, Berlin, 1984.
- L. I. Rubinstein, The Stefan Problem, American Mathematical Society, Providence, RI, 1971.
- W. W. Mullins and J. P. Hirth, J. Phys. Chem. Solids 24, 1391 (1963).
- R. Ghez, results presented at the Thirty-Second Physical Electronics Conference, Albuquerque, NM, March 20–22, 1972.
- 39. K. Voigtlaender, H. Risken, and E. Kasper, Appl. Phys. A 39, 31 (1986). Aleksandrov and Entin [28] had solved the same problem, but their solution for nonequilibrium steps is incorrect because they neglected the convection terms in the Stefan condition (6).
- 40. V. Fuenzalida and I. Eisele, J. Cryst. Growth 74, 597 (1986).
- 41. G. Ehrlich and F. G. Hudda, J. Chem. Phys. 44, 1039 (1966).
- 42. S.-C. Wang and T. T. Tsong, Surf. Sci. 121, 85 (1982).
- 43. H.-W. Fink and G. Ehrlich, Surf. Sci. 143, 125 (1984); 173, 128 (1986).
- 44. It is true that these FIM studies deal with surfaces of refractory metals, but more recent studies suggest that similar work on silicon is possible. See H. M. Liu, T. T. Tsong, and Y. Liou, Phys. Rev. Lett. 58, 1535 (1987); H. M. Liu and T. T. Tsong, J. Appl. Phys., 62, 1532 (1987).
- 45. In the MBE of Si, the flux F incident on terraces is indistinguishable from the flux, at the substrate location, that is created by the e-beam evaporator. For other cases, such as the

- MBE of GaAs, the expression for F may contain sticking coefficients or coverage factors.
- 46. This dimensionless combination (or more precisely, its inverse) is sometimes known, in the chemical engineering literature, as the "Damköhler number."
- 47. In view of definition (1), this diffusion velocity D_s/x_s is also x_s/τ_s .
- 48. Recall that the symbol \(\ell\), unless otherwise stated, denotes the dimensionless \(\ell/\chi_*\).
- 49. There is here a fundamental difference with BCF-like models that neglect convection of steps: The function f(V) can be greater than unity. See, for example, Equation (22), and note that the distance between steps is not bounded.
- 50. Schwoebel's concentration distribution, valid for low $\sigma\theta_e$, is a special case, when $V \rightarrow 0$, of Equations (13) and (14).
- 51. By "large" step distances we mean distances / that are large compared to the mean diffusion distance x_e , and not merely large compared to the lattice distance a. In that case, steps do not interact significantly through the surface diffusion field. Driving forces $\sigma\theta_e$, however, are considered "large" when compared to unity.
- S. S. Iyer, R. A. Metzger, and F. G. Allen, J. Appl. Phys. 52, 5608 (1981).
- 53. Y. Ota, Thin Solid Films 106, 1 (1983).
- E. Kasper and K. Wörner, in Proceedings of the 2nd Symposium on VLSI Science and Technology, K. E. Bean and G. A. Rozgonyi, Eds., Electrochemical Society, Pennington, NJ, 1984, Vol. 84-7, pp. 429-447.
- 55. F. G. Allen, Thin Solid Films 123, 273 (1985).
- 56. J. C. Bean, Science 230, 127 (1985).
- S. Delage, P. A. Badoz, E. Rosencher, and F. Arnaud d'Avitaya, Electron. Lett. 22, 207 (1986).
- S. S. Iyer, in *Epitaxial Silicon Technology*, B. J. Baliga, Ed., Academic Press, Inc., New York, 1986.
- T. De Jong, Ph.D. Dissertation, University of Amsterdam, Netherlands, 1983.
- 60. E. Kasper, Appl. Phys. A 28, 129 (1982).
- 61. H. A. Wilson, Phil. Mag. 50, 238 (1900).
- 62. J. Frenkel, Phys. Z. Sowjetunion 1, 498 (1932).
- 63. The following discussion is independent of those factors that control the distance between steps \(\textit{.} \) For concreteness, however, we will now interpret step trains as due to wafer misorientation. Consequently, the words "step distance," "step density," and "misorientation" are used interchangeably.
- T. Sakamoto, N. J. Kawai, T. Nakagawa, K. Ohta, and T. Kojima, *Appl. Phys. Lett.* 47, 617 (1985).
- T. Sakamoto, T. Kawamura, S. Nago, G. Hashiguchi, K. Sakamoto, and K. Kuniyoshi, J. Cryst. Growth 81, 59 (1987).
- J. Aarts, W. M. Gerits, and P. K. Larsen, Appl. Phys. Lett. 48, 931 (1986).
- 67. This is exactly the parameter b of [39].
- 68. These numbers differ slightly from similar numerical estimates reported elsewhere (cf. [39, 60]) because of the way in which the data of Honig and Kramer [71] were fitted and because of Equation (C5).
- 69. J. H. McFee, R. G. Swartz, V. D. Archer, S. N. Finegan, and L. C. Feldman, J. Electrochem. Soc. 130, 214 (1983).
- 70. R. Ghez, Surf. Sci. 20, 326 (1970).
- 71. R. E. Honig and D. A. Kramer, RCA Rev. 30, 285 (1969).
- 72. M. Ichikawa and T. Doi, Appl. Phys. Lett. 50, 1141 (1987).
- S. S. Iyer, T. F. Heinz, and M. M. T. Loy, J. Vac. Sci. Technol. B 5, 709 (1987).

Received July 1, 1987; accepted for publication March 15, 1988

Richard Ghez IBM Research Division, T. J. Watson Research Center, P.O. Box 218, Yorktown Heights, New York 10598. Dr. Ghez received his Ph.D. from the Ecole Polytechnique in Lausanne, Switzerland, in 1967. In 1970, after postdoctoral work at the University of Virginia, he joined IBM as a Research Staff Member at the IBM T. J. Watson Research Center. He is an Associate Editor of the Journal of Crystal Growth, and a member of the Executive Committee of the American Association of Crystal Growth. His book, A Primer of Diffusion Problems, was recently published by John Wiley & Sons.

Subramanian S. lyer IBM Research Division, T. J. Watson Research Center, P.O. Box 218, Yorktown Heights, New York 10598. Dr. lyer received a B.Tech. in electrical engineering from the Indian Institute of Technology, Bombay, in 1977, and an M.S. and Ph.D. from the University of California at Los Angeles in 1978 and 1981, respectively. Since 1981, he has been a Research Staff Member at the IBM T. J. Watson Research Center. He has worked on electromigration in submicron metal lines and has developed processes for chip metallization. His current interests are in the growth and doping mechanisms in silicon-based molecular beam epitaxy, and exploratory device applications of low-temperature epitaxial processes.